ISSN 1674-1056
http://cpb.iphy.ac.cn
http://iopscience.iop.org/cpb
中国物理 B
Chinese Physics
中国物理
Chinese Physics B

Optical characterization of defects in narrow-gap HgCdTe for infrared detector applications

Fang-Yu Yue(越方禹), Su-Yu Ma(马骕驭), Jin Hong(洪进), Ping-Xiong Yang(杨平雄), Cheng-Bin Jing(敬承斌), Ye Chen(陈晔), Jun-Hao Chu(褚君浩)

Citation: Chin. Phys. B . 2019, 28(1): 017104. **doi:** 10.1088/1674-1056/28/1/017104
Journal homepage: http://cpb.iphy.ac.cn; http://iopscience.iop.org/cpb

What follows is a list of articles you may be interested in

Electronic structures of impurities and point defects in semiconductors

Yong Zhang(张勇)
Chin. Phys. B . 2018, 27(11): 117103. **doi:** 10.1088/1674-1056/27/11/117103

Characteristic modification by inserted metal layer and interface graphene layer in ZnO-based resistive switching structures

Hao-Nan Liu(刘浩男), Xiao-Xia Suo(索晓霞), Lin-Ao Zhang(张林奥), Duan Zhang(张端), Han-Chun Wu(吴汉春), Hong-Kang Zhao(赵宏康), Zhao-Tan Jiang(江兆潭), Ying-Lan Li(李英兰), Zhi Wang(王志)
Chin. Phys. B . 2018, 27(2): 027104. **doi:** 10.1088/1674-1056/27/2/027104

Cubic ZnO films obtained at low pressure by molecular beam epitaxy

Wang Xiao-Dan, Zhou Hua, Wang Hui-Qiong, Ren Fei, Chen Xiao-Hang, Zhan Hua-Han, Zhou Ying-Hui, Kang Jun-Yong
Chin. Phys. B . 2015, 24(9): 097106. **doi:** 10.1088/1674-1056/24/9/097106

Experimental and theoretical study on field emission properties of zinc oxide nanoparticles decorated carbon nanotubes

Li Xin, Zhou Wei-Man, Liu Wei-Hua, Wang Xiao-Li
Chin. Phys. B . 2015, 24(5): 057102. **doi:** 10.1088/1674-1056/24/5/057102

Defect properties of $CuCrO_2$: A density functional theory calculation

Fang Zhi-Jie, Zhu Ji-Zhen, Zhou Jiang, Mo Man
Chin. Phys. B . 2012, 21(8): 087105. **doi:** 10.1088/1674-1056/21/8/087105

TOPICAL REVIEW — Photodetector: Materials, physics, and applications

Optical characterization of defects in narrow-gap HgCdTe for infrared detector applications*

Fang-Yu Yue(越方禹)[1,†], Su-Yu Ma(马骕驭)[1], Jin Hong(洪进)[1], Ping-Xiong Yang(杨平雄)[1], Cheng-Bin Jing(敬承斌)[1], Ye Chen(陈晔)[1], and Jun-Hao Chu(褚君浩)[1,2]

[1] *Key Laboratory of Polar Materials and Devices (MOE), Department of Optoelectronics, School of Information Science Technology, East China Normal University, Shanghai* 200241, *China*

[2] *National Laboratory for Infrared Physics, Shanghai Institute of Technical Physics, Chinese Academy of Sciences, Shanghai* 200083, *China*

(Received 17 October 2018; revised manuscript received 14 November 2018; published online 12 December 2018)

Narrow-gap $Hg_{1-x}Cd_xTe$ material with a composition x of about 0.3 plays an extremely important role in mid-infrared detection applications. In this work, the optical properties of doped HgCdTe with $x \approx 0.3$ are reviewed, including the defects and defect levels of intrinsic V_{Hg} and the extrinsic amphoteric arsenic (As) dopants, which can act as shallow/deep donors and acceptors. The influence of the defects on the determination of band-edge electronic structure is discussed when absorption or photoluminescence spectra are considered. The inconsistency between these two optical techniques is demonstrated and analyzed by taking into account the Fermi level position as a function of composition, doping level, conductivity type, and temperature. The defect level and its evolution, especially in As-doped HgCdTe, are presented. Our results provide a systematic understanding of the mechanisms and help for optimizing annealing conditions towards p-type As-activation, and eventually for fabricating high performance mid-infrared detectors.

Keywords: HgCdTe, defects, annealing procedures, optical characterization

PACS: 71.55.–I, 71.55.Gs, 78.55.–m, 61.72.Cc **DOI:** 10.1088/1674-1056/28/1/017104

1. Introduction

The importance of the variable band gap $Hg_{1-x}Cd_xTe$ semiconductors for infrared detection is well known; e.g., the small composition HgCdTe material with $x \leq 0.3$ still plays an extremely important role in fabricating mid-infrared focal plane arrays or multi-color detectors and may keep this status in the future.[1,2] For high-quality HgCdTe devices, the realization of p-type doping (or conductivity) is vital and has received much attention during the past few decades.[3,4] A direct and straight forward technique in which intrinsic p-type conductivity is realized by the cation metal vacancy V_{Hg}-doping as shallow acceptors is the most desirable. This is implemented during the growth of bulk material or by liquid phase epitaxy (LPE). However, V_{Hg} is also known to act as Shockley–Read–Hall recombination centers for minority carriers, thus shortening the carrier lifetime and reducing the quantum efficiency of detectors with p-type photon absorption layers. This, on the one hand, limits the effective p-type carrier density (typically below $\sim 10^{18}$ cm^{-3}) and, on the other hand, degrades the crystal quality if the p-type conductivity level rises by increasing the intrinsic cation vacancy concentration.

In this case, the p-type conductivity implemented by extrinsic p-type doping in HgCdTe becomes more and more favorable and has been extensively investigated with the goal of fabricating large scale high performance infrared detector focal plane arrays. Until to now, the column V elemental arsenic (As) is thought as the most favorite dopant, mainly because of its stability and low diffusivity in HgCdTe, which is related to the best device performance parameters.[5,6] Another important advantage is involved in the growth method of *in situ* As-doping in HgCdTe by the molecular beam epitaxy (MBE), which can avoid high Hg pressures and lattice imperfections.[7] However, the As dopant in HgCdTe is electrically amphoteric. Under metal-rich condition it can be incorporated as an acceptor as As_{Te} (As occupies the Te site), while it is incorporated as a donor as As_{Hg} (As occupies the Hg site) under Te-rich growth condition.[7,8] Thereafter, a post-growth annealing process, especially a two-stage annealing process, has been proposed to realize extrinsic p-type conductivity. This takes place by transferring the As from occupying Hg-sublattice sites to Te-sublattice sites under low activation temperature (e.g., < 300 °C) for preserving the intrinsic advantages of the low growth temperature of MBE. Different activation annealing processes on As-doped HgCdTe have been investigated by using different growth technologies, theoretical calculations, electrical measurements, and optical methods such as in our previous researches by modulating photolumi-

*Project supported by the Major Program of the National Natural Science Foundation of China (Grant Nos. 61790583, 61874043, 61874045, and 61775060) and the National Key Research and Development Program, China (Grant No. 2016YFB0501604).

†Corresponding author. E-mail: fyyue@ee.ecnu.edu.cn

© 2019 Chinese Physical Society and IOP Publishing Ltd

nescence (PL) and photoreflectance (PR).[9–11] However, it is difficult to reach a consistent result on: (i) the optimized annealing condition, (ii) the physical mechanism relating to a low activation temperature, (iii) the defect activation energies, and (iv) the origin of As when GaAs is employed as the substrate.

Precise knowledge about the key parameters (such as the optical bandgap E_g) of doped-HgCdTe is a prerequisite for developing high quality devices. To obtain the most important optical bandgap value E_g of the materials, intrinsic absorption and transmission spectra are frequently analyzed, usually at a temperature of 77 K (liquid nitrogen temperature) or 300 K (room-temperature);[12] or for devices, the cutoff wavelength obtained from photocurrent (PC) spectra at room temperature is analyzed. Accordingly, the composition (x) can be deduced by using empirical formulas, e.g., CXT by Chu *et al.*[13] or HSC by Hansen *et al.*,[14] which work for a given sample if E_g changes linearly with temperature. Experimentally, the intrinsic absorption spectrum is determined by Fourier transform infrared (FTIR) spectroscopy that is regarded as a classical, straightforward, and accurate way to evaluate the optical E_g of HgCdTe. In such measurements, a non-linear shift of the absorption edge was observed with temperature in all kinds of doped HgCdTe, including material intrinsically or extrinsically doping. This suggests that the defects in HgCdTe influence the absorption edge and an extrinsic absorption edge is generated by contributions of defect-related transitions. This subsequently affects the determination of E_g (as well as the x value) of HgCdTe.

As mentioned previously, PL spectroscopy provides an effective way to investigate the band-edge electronic structure of doped-HgCdTe including the so-called PL bandgap (E_g^{PL}). It should be mentioned that for narrow-gap HgCdTe, standard PL setups show limitations to directly investigating E_g^{PL} and defect levels, which is most likely due to the room-temperature background radiation signal (RT-BG) located in the mid-infrared range around 10 μm. It largely influences the collection and extraction of the weak infrared PL signals of HgCdTe. Under these circumstances, the mathematical procedure of subtracting the RT-BG, or technical methods including double-modulation and the phase-sensitive detection based on the rapid-scan or step-scan of the FTIR in concert with a lock-in amplified detection system, have been adopted.[15] Some defect-related optical parameters including the extrinsic-As and the intrinsic-V_{Hg} as well as the tellurium antisite (Te_{Hg}) have been determined for As-doped HgCdTe. However, it should be emphasized that E_g^{PL} frequently deviates from E_g, i.e., there is a Stokes shift (E_s) that is frequently observed in low-dimensional materials. Although the reason for this deviation in HgCdTe has been extensively investigated based on some assumptions, such as an Urbach tail of states or excitonic effects,[16] only a few reports about the influence of the defects have been published, particularly when the Stokes shift shows a non-monotonic evolution with temperature. These phenomena demonstrate that the temperature acts as a key parameter in determining the band-edge electronic structure including the derivation of x-value in intrinsic/extrinsic-doped HgCdTe when both absorption and PL spectra are employed.

In this work, we review the optical properties of V_{Hg}- or As-doped HgCdTe with $x \sim 0.3$, grown by different methods including bulk growth, LPE, and MBE. Absorption and PL spectra at different temperatures are used to analyze the optical bandgaps (E_g and E_g^{PL}) and the defect levels. The results are used to optimize the annealing conditions to fully activate the doped As as shallow acceptors in the HgCdTe. The observed Stokes shifts with temperature and the mechanisms behind are presented and discussed by referring to the Fermi level position (E_F) as a function of x, conductivity type (p or n), doping level, and temperature. Consequently, the band-edge electronic level structure including the defect levels in the As-doped material system is schematically demonstrated for different growth or annealing conditions. These results give a systematical understanding of the optical properties of doped HgCdTe and provide guidance to obtain As-activated p-type HgCdTe as well as for fabricating high-performance HgCdTe infrared detection devices.

2. Sample and experimental details

The samples used in this work include V_{Hg}-doped HgCdTe grown as bulk material, by LPE and MBE, and As-doped HgCdTe grown by MBE. For As-activation, different annealing conditions have been used. The main composition of the samples is $x \sim 0.3$.

The infrared reflectance, absorption, and PL were measured. Variable temperatures (from ~ 8 K to 300 K) were used for absorption and PL measurements. For PL, different excitation densities were applied. As a reference, PC and photoreflectance (PR) results have been used.

2.1. Doped-HgCdTe

Bulk HgCdTe samples were prepared by the Bridgman method. The p-type conductivity is due to intrinsic V_{Hg}, leading to a carrier density on the order of 10^{14} cm^{-3} at 77 K. The corresponding carrier mobility was on the order of 10^4 $cm^2/V{\cdot}s$. The thickness of the samples was determined by a micrometer gauge with a standard thickness of less than 500 μm.

The LPE samples were V_{Hg}-doped by using a reflux vertical impregnation LPE system, which allows to grow big-area, compositional uniform, good surface profile epilayers with a controllable pressure of the solution. The substrates of the epilayers were (111) surfaces of CdTe or CdZnTe (~ 4% of Zn),

the latter was for the purpose of lattice match. The surface area was about 18 mm×20 mm. The substrate was fixed by a clamp with a vertical inlet and outlet way. In a horizontal growth process, both the drop and pull-up of the sample were in vertical direction, while the growth direction was horizontal. The horizontal growth made the composition and thickness of the epitaxial layer uniform, while the vertical separation from the growth solution reduced the adhesion of any mother solution. After growth, the samples were annealed at different temperatures and times under Hg-rich condition. The p-type conductivity at 77 K was due to V_{Hg}, leading to a carrier density on the order of 10^{15} cm^{-3}. The LPE samples L1–L6 were used for analysis. Among them, the main differences were the x value, the thickness, and, of course, the carrier density and mobility. The thickness of the HgCdTe layer was evaluated based on the Fabry–Pérot interference in the transmission spectra and was typically 10 μm.

The MBE-grown HgCdTe epilayers were grown in a Riber 32P MBE system on undoped semi-insulating GaAs (211)B substrates. A CdTe buffer layer 3 μm in thickness was grown prior to the HgCdTe nucleation. For comparison, As-doped and V_{Hg}-doped MBE samples were prepared. Except for the as-grown reference epilayer without any annealing, the other samples were annealed including a single- or two-stage annealing process, where the latter (e.g., 285 °C/0.5 h +240 °C/48 h) was known to be beneficial to the As-activation without other residents. This happens because the first stage pushes the As from Hg sites to Te sites and the second stage, with a relatively low temperature, can remove the excess V_{Hg} and avoid forming the n-type As_{Hg}.[17,18] The details of the samples are listed in Table 1, including composition and thickness, as well as the carrier concentration.

Table 1. Composition (x), thickness (d), carrier density (N_c), mobility (M_c), and nature of defects in MBE samples.

	x	d/μm	$N_c^{77\ K}/10^{15}$	$M_c^{77\ K}/10^3$	Defects	Annealing/(°C/h)
M0	0.300	6.0	12.30	0.26	V_{Hg}, As_{Hg}	as-grown
M1	0.308	7.9	–9.50	–2.82	As_{Hg}	240/48
M2	0.300	5.9	32.70	0.30	As_{Te}	285/0.5+240/48
M3	0.300	11.0	10.10	0.26	V_{Hg}	285/0.5+240/48
M4	0.305	6.1	36.40	0.29	As_{Te}, V_{Hg}	440/0.5+240/48
M5	0.225	10.7	32.00	0.31	V_{Hg}	as-grown

2.2. Optical measurement

Characterization by optical absorption was performed by using a Bruker IFS 66v/S spectrometer, which was equipped with a KBr beam splitter and a liquid-nitrogen-cooled HgCdTe detector. The spectrometer was evacuated during the measurement to avoid any influence of infrared absorption lines in air.

PL spectra were recorded with this setup by using the step-scan option of the FTIR as described elsewhere in detail.[15] The 514.5 nm line of a mechanically chopped (1.8 kHz) Ar^+ laser was used to irradiate the sample with a beam diameter of ∼ 200 μm.

Before the experiment, the samples were treated with a quick etch in a 1% Br_2/methanol solution to avoid influencing the surface smear, and then mounted on the cold finger of an Oxford closed-cycle cryostat. The temperature was adjusted from ∼ 8 K to 300 K. The spectral resolution was set to be 6 cm^{-1} or 0.7 meV.

3. Optical characterizations

3.1. Transmission spectral results

Figures 1(a)–1(c) show the transmission spectra of bulk, LPE, and MBE samples, respectively, which are recorded at low temperature of ∼ 8 K. The samples show high transmittance at the low energy side and relatively steep absorption feature when the photon energy is close to or become higher than the optical E_g. The epitaxial samples demonstrate that the strong interference fringes on the low energy side, i.e., the uniform (or single) pattern, for LPE are due to the interfacial reflectance between the HgCdTe layer and the substrate. The more complex patterns for the MBE sample are caused by the buffer layer between the HgCdTe layer and the substrate. Based on the interference energy distances, the HgCdTe epilayer thickness can be evaluated, as shown in Table 1.

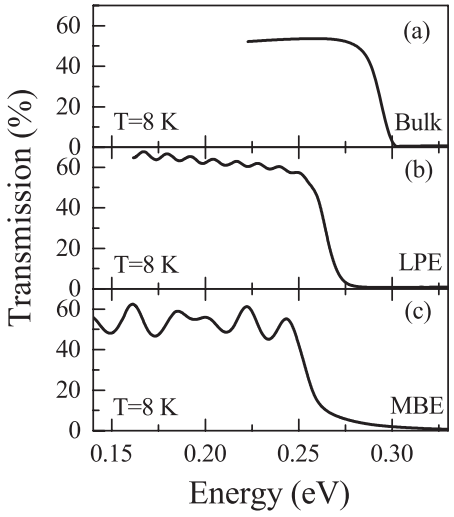


Fig. 1. Transmission spectra of (a) bulk, (b) LPE, and (c) MBE samples at ∼ 8 K.

According to the transmission spectra at any temperature, one can obtain the optical E_g value of HgCdTe. However, when the sample is doped, it can be imagined that the defects can be activated thermally and the carrier density is determined by the doping level and the temperature. This suggests that the absorption process of the carriers in the doped samples should be different from that without doping, on which transmission measurements are often considered to provide the intrinsic absorption spectra.

Figure 2 shows the transmission spectra of the three samples at different temperatures. At first glance, the absorption edge seems to blue-shifted as the temperature increases. It is, however, important to mention that for the three samples, the absorption edge does not monotonically blue-shift but presents an S-shaped evolution in the low temperature range. First, it blue-shifts with the temperature increasing from the lowest value but then red-shifts as the temperature exceeds a certain value (e.g., $\sim$ 33 K for bulk, $\sim$ 50 K for LPE, and $\sim$ 30 K for MBE), and reaches the lowest energy point at $\sim$ 55 K, 67 K, and 70 K for the bulk, LPE, and MBE samples, respectively. Thereafter, the absorption edge moves monotonically up to 300 K. In other words, the evolution of the absorption edge is abnormal when the temperature is in a range of about 30–70 K. It is worthwhile emphasizing that the spectra of all of the other samples show similar temperature dependence with the exception of n-type MBE sample,[19–21] which shows a monotonic temperature dependence of the absorption edge in the whole temperature range. Although the critical temperature points are different for different samples, the temperature is below 77 K.

From the transmission spectra given in Figs. 1 and 2, the corresponding absorption-coefficient α spectra can be deduced and are shown in Fig. 3.[20] The x value can then be deduced from the spectra. Here, we first obtain the results at the lowest temperature of $\sim$ 8 K from the following absorption coefficient expression:[22]

$$\alpha_{E_g} = -65 + 1.88T + (8694 - 10.31T)x. \quad (1)$$

Because of the difference in α values between the bulk and epilayer due to the thickness difference of HgCdTe, different procedures should be undertaken for these two kinds of samples in order to determine the critical point on the absorption spectrum. For the bulk samples with a thickness on the order of submillimeters, the absorption coefficient is extrapolated to the α_{E_g} as the critical point (Fig. 3(a)). For the epilayers having a thickness on the order of μm, the energy point is determined as the critical value at the cross point between the plateau and exponential region (Figs. 3(b) and 3(c)). Note that the non-monotonic shift of the absorption edge on the low temperature side is still present.

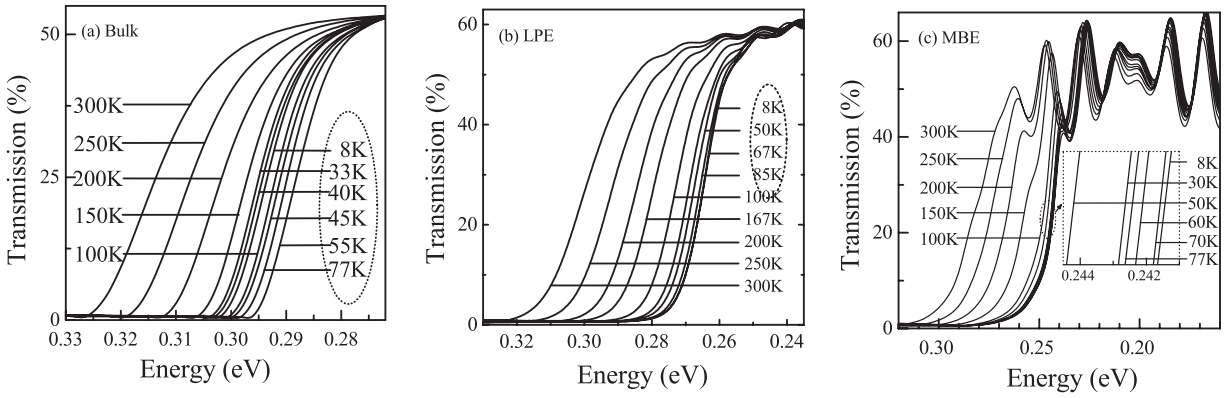


Fig. 2. Transmission spectra of (a) bulk, (b) LPE, and (c) MBE samples at different temperatures.

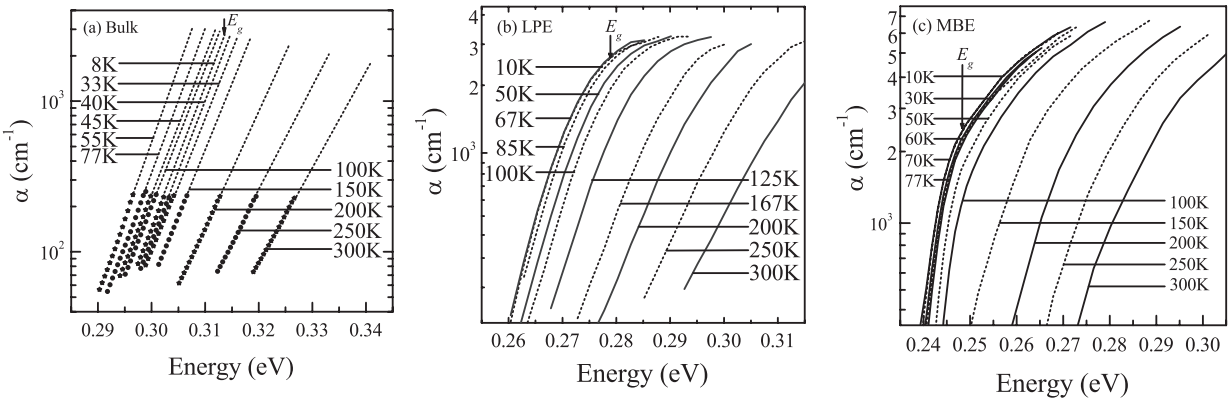


Fig. 3. Absorption coefficient spectra of (a) bulk, (b) LPE, and (c) MBE samples at different temperatures.

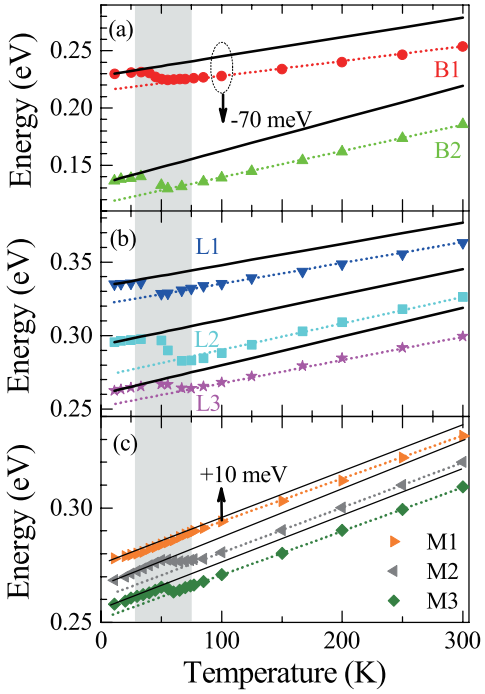


Fig. 4. Representative temperature-dependent E_g values for (a) bulk, (b) LPE, and (c) MBE samples. Part of the data have been up- or down-shifted for clarity. The solid lines are predicted by CXT to guide the eyes.

Figure 4 summarizes the determined E_g values for all samples by referring to the α_{E_g} values at different temperatures.[20] The $E_g \sim T$ evolution predicted by the CXT empirical expression is also shown for each sample to guide the eyes[23]

$$E_g(x,T) = -0.295 + 1.87x - 0.28x^2 + 0.35x^4 + (6 - 14x + 3x^2) \times 10^{-4} T. \quad (2)$$

The consistent x value can be calculated by referring to the absorption coefficient spectra at any temperature point and Eq. (2). However, due to the existence of the abnormal shift of the absorption edge, the referenced temperature point becomes a key issue for determining the exact x value. Here, we tentatively extract the value based on the result of the lowest temperature; e.g., $\sim$ 10 K. The reason and details will be discussed in the following.

As shown in Fig. 4, the absorption-edge energy is blue-shifted in the entire temperature range, but there exists a non-monotonic shift in the low temperature range, marked by the shadowed area. A red-shift can be observed except for the n-type epilayer sample. Since the x value is determined based on the result of $\sim$ 10 K, the predictions from the empirical expression match well with the experimental data from the low temperature side, but on the high temperature side they deviate evidently from each other. Note that although the n-type MBE sample does not show any redshift in the shadowed area, the evolution of the experimental data is slower than that of Eq. (2); i.e., with a smaller slope than the dE_g/dT value. In this case, extrapolating the linear region downwards the high temperature part, there should be an energy separation ΔE at 0 K (but not for the n-type samples).[24] No doubt, based on one of the two evolution data, the determined x value should be inconsistent for a certain sample. Another important phenomenon should be pointed out that the deviation in V_{Hg}-doped samples (including the bulk, LPE, and MBE samples) gives a slightly bigger ΔE value than that of the As-doped MBE samples (including the p-type and, of course, n-type samples).

3.2. PL results

Figure 5(a) shows the PL spectra of several LPE samples at 8 K, which are unintentionally doped. The spectra show more than one PL peak. Curve fits demonstrate two separated peaks, the high energy peak named A_0 and the low energy peak B_0 with an energy separation of $\sim$ 14 meV (Fig. 5(b)). To reliably determine the peak positions, the second derivative procedure is adopted in Fig. 5(b), which gives an error of $\sim$ 1 meV as compared with that of the curve fit technique.[25] This shows that the peak position can be accurately determined by both approaches. As for the sample at the bottom of Fig. 5(a), which shows that the PL peaks shift towards the long wavelengths up to $\sim$ 11 μm, the signal-to-noise ratio (SNR) of the spectrum is relatively poor, even under a high excitation power, which is possibly due to the poor quality of the sample with a relatively small $x \sim 0.235$. However, two PL peaks are also evident. The curve fit procedure is done as shown in Fig. 5(c) for different temperatures. The energy separation between the two peaks is also close to that observed for the other samples. For high temperatures, at which a much higher excitation density is necessary, thermal effects induce the broadening of the spectra, particularly towards the high energy side.

PL measurements have been performed at different excitation power and temperatures. Figure 6 summarizes the results of the fit parameters including the peak energy and the integral intensity (I.I.). In Fig. 6(a), there is a blue-shift of both peak energies with the excitation power increasing, especially at high excitation power. This behavior can be interpreted by band filling in the narrow-gap HgCdTe, and on the high excitation power side by the thermal effect, which can make the peak energy blue-shifted due to the positive temperature coefficient of the bandgap (i.e., dE_g/dT) in HgCdTe with a small x. The thermal effect is also confirmed by the relationship between I.I. and excitation power in Fig. 6(b), where the I.I. almost linearly increases first, then becomes saturated (peak A_0) or even decreases (peak B_0) as the excitation power increases.

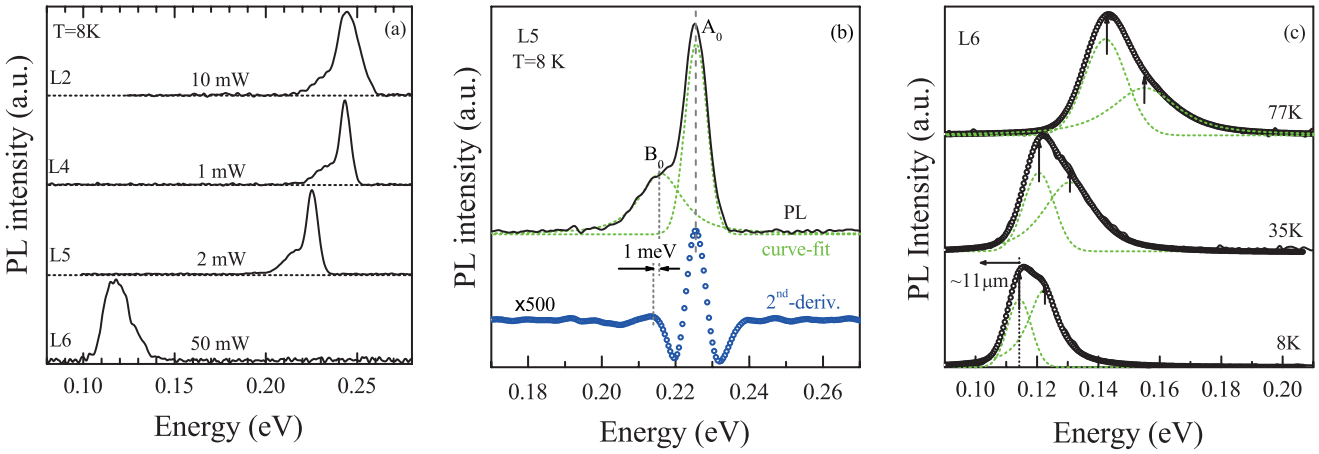


Fig. 5. (a) PL spectra of LPE samples at ∼ 8 K, (b) curve fit and the second derivative procedures applied to the PL spectrum of sample L5, and (c) PL spectra and curve fit results of sample L6 at different temperatures.

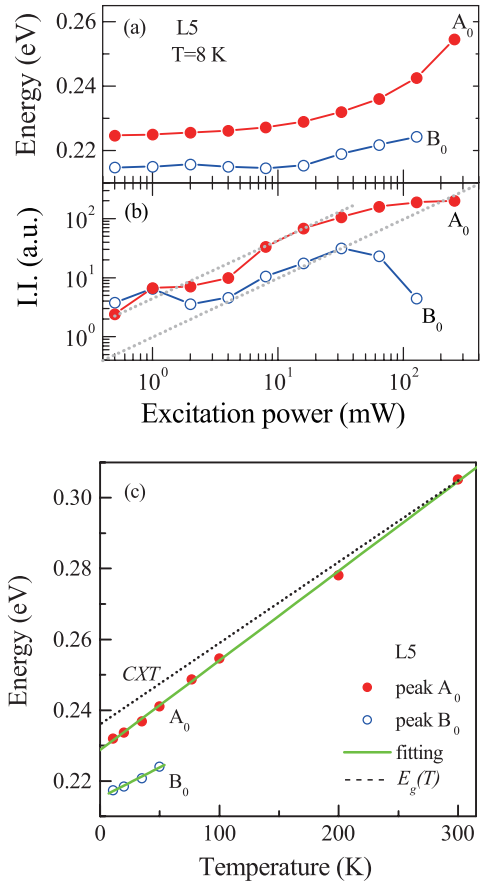


Fig. 6. (a), (b) Excitation power and (c) temperature dependence of the fit parameters obtained from the PL spectra.

Figure 6(c) further gives the temperature dependence of the peak energy. As a comparison, the predicted results of the CXT expression, i.e., Eq. (2), have been added to the figure. Considering the potential excitonic effects and band-tail states in narrow-gap HgCdTe, which frequently induce a redshift of the PL energy as compared with the intrinsic absorption results, the CXT results are given based on the PL energy at a high temperature (300 K). From the figure, we can see that in the entire temperature range, peak A_0 has always a nearly linear blue-shift with temperature increasing, while peak B_0 shows a similar blue-shift but only at low temperatures. Here it is not difficult to attribute the high energy peak A_0 to the band-to-band transition (i.e., E_g^{PL}), since no higher energy peak is observed in the entire excitation and temperature range. The low energy peak B_0 represents a defect-related behavior. The V_{Hg} shallow defect could be responsible by taking into account the energy separation from peak A_0, and the facts that (i) the relative intensity of peak B_0 to peak A_0 decreases but does not change its spectral shape as the excitation power increases, and (ii) the V_{Hg}-doping of the samples. Thereafter, it can be estimated that the V_{Hg} has an activation energy of ∼ 14 meV, which is consistent with the results reported from electronic and optical experiments, as well as theoretical predictions. Note that the relation between the peak A_0 energy and temperature shows a steeper slope (i.e., dE_g/dT) than that of CXT, and that the defect activation energy related to V_{Hg} is close to the abnormal shift ΔE value in the absorption measurement.

Now we come to the As-doped samples, which are grown by MBE. Figure 7(a) shows the PL spectrum of the as-grown sample at 8 K. It is an extremely complex PL spectrum with multiple peaks, including a pronounced part on the high energy side and the relatively weak part on the low energy side. Curve fits reveal more than seven peaks, which can be divided into two groups: one for peaks *A*–*E* and the other for peaks *F* and *G*. Between them exists an energy difference up to ∼ 90 meV. For comparison, figure 7(b) shows the PL spectrum of an annealed sample at the same temperature, to which an optimized two-stage process (see Table 1) is applied in order to fully activate the doped-As in HgCdTe.[11] Indeed, this spectrum shows a relatively simple shape, similar to those of the V_{Hg}-doped samples in Fig. 5. Curve fits give two peaks separated by an energy difference of less than 12 meV. The band-to-band peak is increased at the cost of the defect-related transitions. It should be emphasized that comparing with the spectral shape of the as-grown sample, an annealing process

can optimize the spectral shape, and at the same time also eliminate the PL signals on the low energy side.

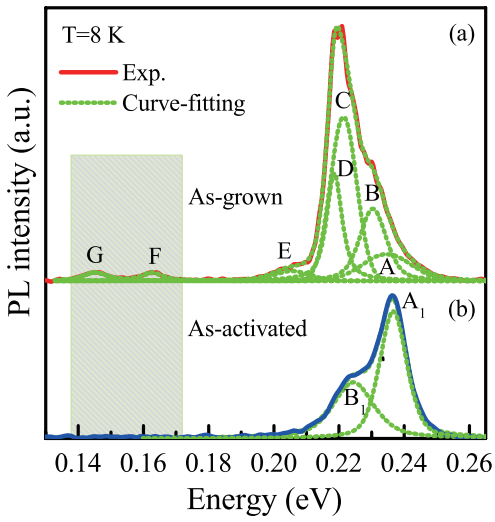


Fig. 7. Representative PL spectra of (a) as-grown sample M0 and (b) As-activated annealed sample M2 at ∼ 8 K, and their line-shape fits. The samples are grown by MBE.

Figure 8 shows the excitation power and temperature dependent PL spectra and the corresponding results of a peak analysis of the annealed sample from Fig. 7(b). The slight blue-shift of the peak energy in Fig. 8(c) is due to band filling as the excitation power increases. In Fig. 8(d), the competition of the I.I. between the two peaks is clear, but beyond ∼ 40 mW both become saturated and even decrease, which is likely to be related to excitation-induced heating. Note that when peak B_1 first shows a near-linear increase with excitation power increasing, peak A_1 even presents a superlinear dependence (see the double-logarithmic scale). From the temperature-dependent peak energy (Fig. 8(e)) and I.I. (Fig. 8(f)), it is evident that the bandgap-related peak A (E_g^{PL}) shows a linear increase with temperature increasing and has an energy separation of ∼ 12 meV from the defect-related peak B_1. According to the doping and the p-type conductivity of the sample by As-activation annealing, as well as the previous discussion, the defect can be attributed to As_{Te} with an activation energy of ∼ 12 meV. It should be pointed out that for comparison, an MBE reference sample with unintentional doping is also annealed like the sample in Fig. 7(b). A similar two-peak structure can also be observed (not shown here) with an energy separation of ∼ 15 meV. It is related to the activation energy of V_{Hg}, which is close to the foregoing results in the LPE samples. Here, the smaller value of As_{Te} than that of V_{Hg} suggests that the former is shallower than the latter. This could be of benefit to the p-type material preparation and relevant device fabrications.[26–28]

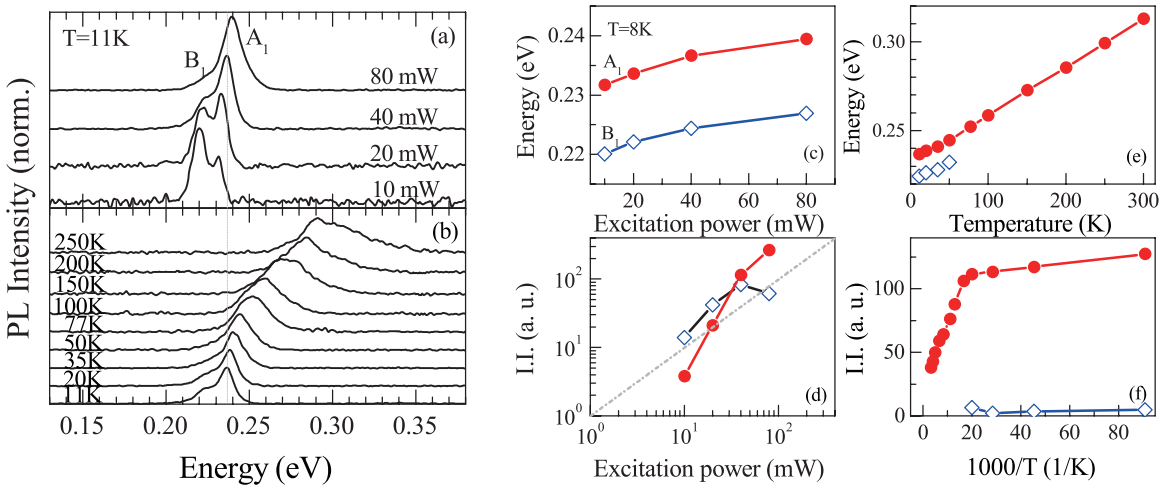


Fig. 8. PL spectra of sample M2 at different excitation powers and temperatures, and (c), (d) excitation power- and (b) temperature-dependent peak energy and peak integral intensity.

To find an optimized annealing process, different annealing procedures are tested. Figure 9 shows the PL spectra of an As-doped MBE sample, which is annealed at a higher annealing temperature (400 °C) during the first-stage as shown in Table 1. As is well known, the Hg–Te binding is extremely weak, and can be broken at a high temperature and therefore low temperature in the entire growth process is required.[28,29] Therefore, a high activation temperature (e.g., ≥ 400 °C) in the first stage produces higher additional V_{Hg} than a low activation temperature (e.g., ≤ 300 °C). From Figs. 9(a) and 9(b), we can see that the PL spectra show four peaks A_2–D_2 compared with those in Fig. 8(a). The excitation power- and temperature-dependent peak energies (obtained by line-shape fitting) show that when A_2 can be ascribed to the E_g-related transition, B_2–D_2 should be defect-related, where the energy differences from A_2 are ∼ 9 meV, 23 meV, and 31 meV, respectively (Figs. 9(c) and 9(d)). Considering the annealing conditions and Berding's theoretical reports,[5,31] the n-type conductivity of this sample suggests not only a dominant As_{Hg} defect, but also the presence of V_{Hg} and complexes of As_{Hg}–V_{Hg}. According to the Sun's theoretical predictions[18,32] and the results obtained previously,[9] peak B_2 can be attributed to an

As_{Hg}-related transition with an activation energy of ~ 9 meV and peak C_2 is related to a V_{Hg}-related transition with an activation energy of ~ 14 meV. Thereafter, peak D_2 that only appears at low temperatures and low excitation densities can be ascribed to the transition related to the As_{Hg}–V_{Hg} complex, because the high temperature and strong excitation could simplify the complex. The energy distance of ~ 8 meV of the complex from the As_{Hg} and V_{Hg} levels discloses its forming energy. Here, we should emphasize that the two-stage annealing process can be used to activate the As with a temperature as low as 285 °C. A higher temperature beyond 300 °C is undesirable from the point of view of defect creation.

After obtaining the specific defect information, the discussion of the origin of abundant peaks in the as-grown sample becomes easier. Figure 10(a) shows the PL spectra of the sample already shown in Fig. 7(a) at different temperatures (up to 100 K).[11] It is obvious that the SNRs of the spectra are relatively poor due to the quality of the epilayer before annealing, especially when the temperature increases. Besides the temperature-dependent evolution of the high energy part (i.e., evident blue-shift of peaks *A*–*E* with temperature), the low energy part (i.e., the deep levels *F*–*H*) shows unusual temperature dependence with competitive occurrence and disappearance of peaks with temperature increasing. For instance, both peaks *G* and *F* are visible at low temperatures, but with the temperature increasing, peak *G* disappears and peak *F* increases, accompanied with the appearance of an additional peak *H*.

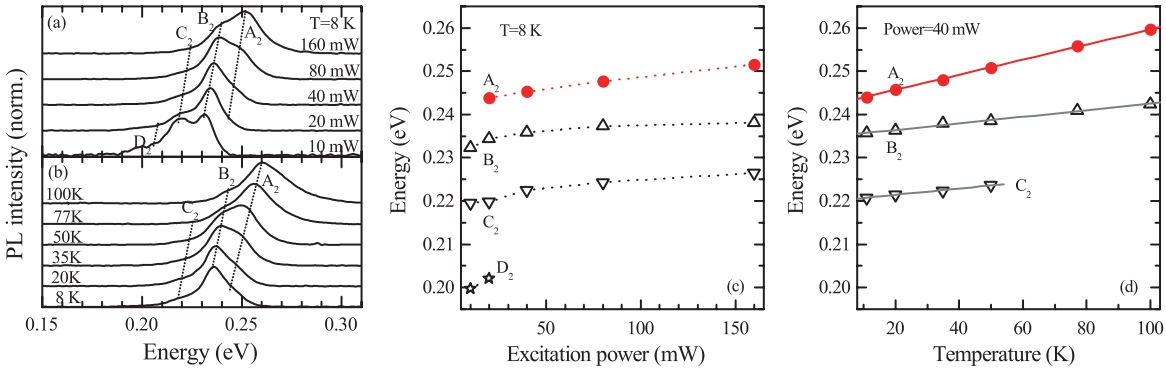


Fig. 9. (a), (b) PL spectra of an As-doped MBE sample (M1) treated with a single-stage annealing process; (c), (d) the peak energies at different excitation powers and temperatures.

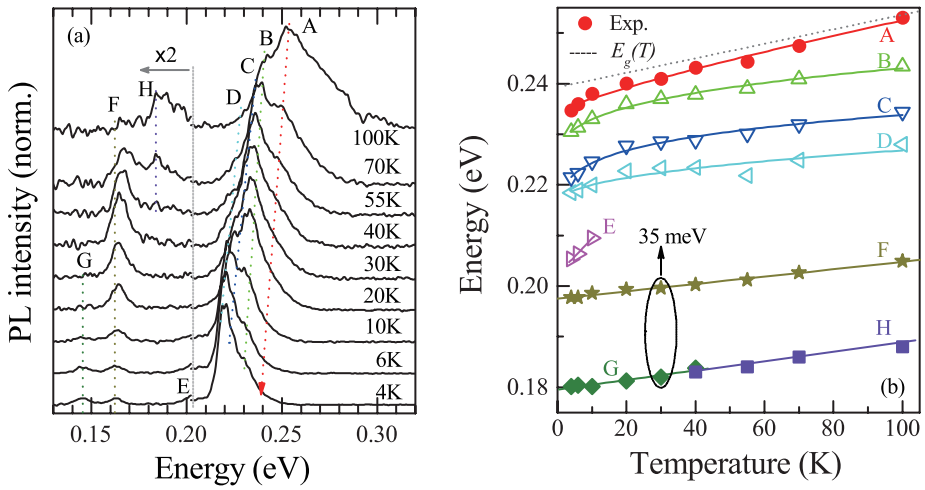


Fig. 10. (a) PL spectra of sample M0 and (b) temperature dependence of the peak energy. For the sake of clarity, the values of *F* and *G* in panel (b) are upshifted by 35 meV.

Figure 10(b) summarizes the peak energies of up to eight peaks *A*–*H* as a function of temperature. For comparison, the results of the CXT formula are shown in the figure. Note that for the as-grown sample, the doped-As should be inactivated, i.e., without occupying the Te lattice sites. Due to the p-type conductivity, the intrinsic V_{Hg} should predominate, and the As is mainly expected to exist as As_{Hg}, which requires a suitable annealing process to transfer from the Hg site to the Te site.[33,34] It needs to be pointed out that the peak number of the fit procedures on the high energy side is based on the previous results, where some values are used, including V_{Hg} ~ 14 meV, As_{Te} ~ 12 meV, As_{Hg} ~ 9 meV, and the As_{Hg}–V_{Hg} complex ~ 31 meV.

It is obvious that the high energy peaks *A*–*D* (maybe *E*,

as well) show a parabolic evolution at low temperatures but as the temperature increases beyond 20 K, they evolve in a linear increase way. The deep-level-related peaks *F*–*H* shift linearly with temperature increasing. The peak positions of *A*–*H* can be determined by extrapolating to 0 K as ∼ 238 meV, 232 meV, 225 meV, 221 meV, 207 meV, 164 meV, 146 meV, and 180 meV, respectively. Obviously, peak *A* has the characteristics of band-to-band transitions, while peaks *B*–*H* are related to defect-related transitions. According to the energy separation of these peaks and the statements given above, the high energy peaks *B*–*E* can be attributed to As_{Hg} (∼ 6 meV), V_{Hg} (∼ 13 meV), Te_{Hg} (∼ 17 meV), and the As_{Hg}–V_{Hg} complex (∼ 31 meV) transitions, respectively. Note that (i) in the unintentionally-doped or the annealed As-doped samples, none of deep levels like peaks *F*–*H* is observed; and (ii) peak *H* only appears at high temperatures and almost overlaps the evolution of peak *G* in the temperature range after the upshift of 35 meV of peak *G*. These may suggest that (i) peaks *F*–*H* should be related to the As dopant, such as the As-related cluster (or perhaps its complex with V_{Hg}) due to the dopant source of As_4, which is prone to form As_i ($i = 1$, 2, and 4) clusters or interstitials in as-grown even by using a thermal cracker cell; and (ii) the deep levels are totally dependent on temperature, showing that the increase can first make the peak *G*-related defect state dissociate and strengthen the intensities of peaks *F* and *H*, and then make the peak *F*-related defect state decomplicated (to the *H*-related defect state) as the temperature increases further. However, obviously, the annealing process can annihilate all of them fully.[11,19]

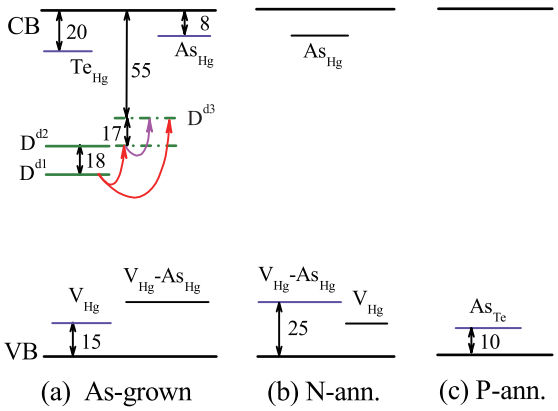


Fig. 11. band-edge electronic structure including defect formation and levels in As-doped HgCdTe for different annealing conditions as determined from our measurements. D^i (i = d1, d2, and d3) represent deep levels. Color arrows depict a dynamic process that D^{d1} can be de-complicated to D^{d2} and D^{d3}, and further from D^{d2} to D^{d3} with temperature increasing.

The band-edge electronic structure in As-doped HgCdTe is schematically summarized in Fig. 11 for the different annealing conditions. In the as-grown samples, the As dopant is on the Hg site and the V_{Hg}–As_{Hg} complex is preferably formed due to the existence of V_{Hg}. At the same time, due to the excess V_{Hg}, the antisite of Te occupying Hg sites can be formed and causes n-type conductivity (or a reversion layer), in particular, at the surface, since the material can be of weakly p-type in conductivity. Obviously, the double deep levels are there, but the origination is pending even though a single deep level has been reported in a theoretical research relating to V_{Hg},[35] because none of the related levels is observed in unintentionally-doped HgCdTe. The n-type annealing process, e.g., at a temperature of 240 °C cannot be useful in removing the V_{Hg} if the As_{Hg} level exists in a certain density because they prefer to form a complex of V_{Hg}–As_{Hg}. It is, therefore, necessary to mention that the two-stage annealing process with a low temperature (down to 285 °C) can effectively activate the As as shallow acceptors with a lower activation energy than that of the intrinsic V_{Hg}.

3.2.1. Stokes shift

As mentioned above, we observe that the absorption edge shifts abnormally with temperature increasing, and the determined E_g is inconsistent with the direct PL result E_g^{PL}, as shown in Fig. 12(a) for an LPE sample. However, it is necessary to point out that the Stokes shift E_s between the results obtained by the two techniques is quite interesting, namely, at 10 K $E_g^{PL} < E_g$ with a normal E_s (about +27 meV) but at high temperatures up to 200 K $E_g^{PL} < E_g$ with a negative E_s, and the absolute value should increase as the temperature increases. That is to say, the Stokes shift has a transition from positive to negative sign.[36]

Details are shown in Figs. 12(b)–12(e), where the temperature-dependent band-edge-related energies and the corresponding E_s are compared. From the figures, we can see that as the PL gives the E_g^{PL}, the defect-related energy can be determined, which is close to the abnormal shift energy of the absorption edge with temperature increasing. Attention should be paid to the E_s as a function of temperature in Figs. 12(d) and 12(e). Here two conceptions about the Stokes shift are defined: the experimental E_s (corresponding to the value of E_g–E_{PL}) and E_s' corresponding to the value of E_{CXT}–E_{PL}. It is evident that both evolutions are dissimilar. While E_s decreases with the temperature increasing, E_s' decreases faster and changes the sign from positive (normal) to negative (abnormal) at a certain temperature point T_s, e.g., ∼ 150 K for the unintentionally doped LPE sample or ∼ 120 K for the As-activated MBE sample. Energetically, they (∼ 13 meV for the former and ∼ 10 meV for the latter) are relatively close to the activation energy of the corresponding defects; i.e., V_{Hg} and As_{Te}, respectively. This may further suggest that the abnormal shift of the Stokes energy is related to the defect levels as discussed in the abnormal shift of the absorption edge energy.

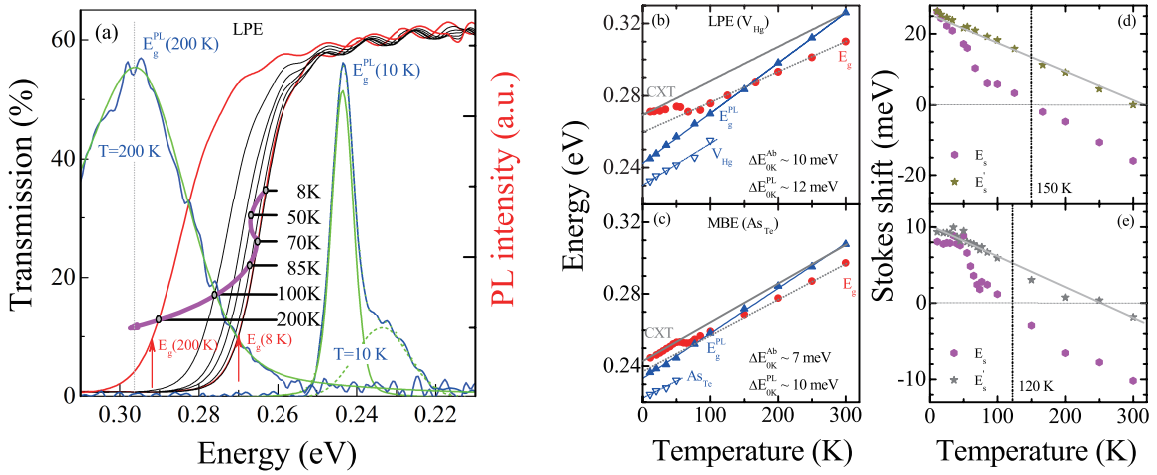


Fig. 12. (a) Comparison between PL and absorption spectra of a representative LPE sample, (b)–(e) plots of temperature-dependent optical bandgap value obtained from absorption and PL spectra, and experimental Stokes shifts.[36] For comparison, the Stokes shifts are also shown according to the CXT formula.

3.2.2. Comparison of the results obtained by different optical techniques

Based on this discussion, it can be imagined that to accurately determine the optical bandgap E_g (on which the x value depends in HgCdTe) is a key issue, because the measurement temperature point plays a vital role for different spectroscopic techniques including the transmission and PL. It involves that the reference temperature is intrinsically dependent on the selected optical method. Thus, to evaluate the accuracy of the determination of the optical E_g, figure 13 comparatively shows the PR and PC spectral results of an unintentionally-doped LPE sample at 77 K. This figure shows the line-shape fit results for PL and PR.[10,37] Note that the fit to the PL spectrum has considered the asymmetry of the spectrum that is due to the thermal broadening.

From this figure, we can see that if the cutoff wavelength (or energy) of the PC spectrum is considered as the value of E_g for the material, the PR spectrum, which can give the fine electronic structure including the defect levels also gives a very consistent value. However, this value is a little blue-shifted as compared with the PL results but a little red-shifted as compared with the transmission results, and this value is used as a standard value to evaluate the optical E_g of semiconductors, where the Stokes shift has a positive coefficient. Note that the PL spectrum at 77 K does not show the defect-related (i.e., V_{Hg}) emission peak, while at a low temperature (10 K), the V_{Hg}-related peak is evident as shown by the first sample (Fig. 5(a)). It should be also mentioned that the evaluated E_g value from the transmission spectrum is smaller than the prediction of the CXT expression, probably due to the existence of the V_{Hg}. From the point of view of the determination of E_g, we can draw a preliminary conclusion that the transmission or absorption measurement can be regarded as a suitable way to evaluate the optical E_g of intrinsic HgCdTe, while for doped-HgCdTe, all of the methods show a red-shift due to the existence of either the defect levels or the band-tail states.

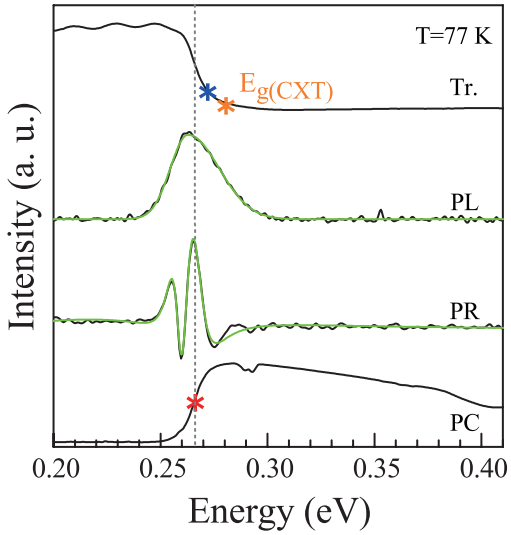


Fig. 13. Determination of optical bandgap E_g in unintentionally-doped HgCdTe sample L2 by different spectroscopic techniques including transmission, PL, PR, and PC at 77 K. Fit results are shown in green. Marked stars refer to corresponding E_g. $E_{g(CXT)}$ is obtained from the CXT expression. Dashed vertical line is used to guide the eyes to E_g obtained by PC.

4. Theoretical calculation of E_F

4.1. Model of E_F for HgCdTe

The Stokes shift E_s exists between the absorption and PL spectra, which are based on the reverse transition process of carriers. Thus, to explain the non-monotonic shift of the absorption edge and subsequently the abnormal shift of E_s as temperature increases, it is vital to determine the position of the Fermi level E_F, which influences the probability of transitions in a certain state. The electrical neutrality condition can be written as follows when considering p-type HgCdTe with only one single acceptor:

$$N_v \exp\left(-\frac{E_F - E_v}{k_B T}\right) = N_c \exp\left(-\frac{E_c - E_F}{k_B T}\right) + \frac{N_A}{1 + g_A \exp\left(-\frac{E_F - E_A}{k_B T}\right)}, \quad (3)$$

with

$$N_c = \frac{2(2\pi m_n^* k_B T)^{3/2}}{h^3}, \quad N_v = \frac{2(2\pi m_p^* k_B T)^{3/2}}{h^3}, \tag{4}$$

where E_c, E_v, E_A, and N_A are the extrema of the conduction (CB) and valence (VB) bands, the shallow acceptor level, and the doping level of acceptors, respectively; k_B is the Boltzmann constant; T is the absolute temperature (K); h is the Planck constant; and $N_{c/v}$ is the effective state density of CB or VB. For doped-HgCdTe ($E_g \gg 2k_BT$), the degeneracy factor $g_A = 4$. The $m_{n/p}$ is the effective mass of electron and hole,[13]

$$m_n^* = 0.05966\frac{E_g(E_g+1)m_0}{E_g+0.667}, \quad m_p^* = 0.55m_0, \tag{5}$$

where m_0 is the rest mass of the electron, and E_g refers to the value shown in Eq. (2).

For comparison with the ionized defects, we calculate the intrinsic density of carriers n_i according to[23]

$$n_i = 5.03\times10^{14}\times\left(1+\frac{3.25k_BT}{E_g}\right)E_g^{3/4}T^{3/2} \times \exp\left(-\frac{E_g}{2k_BT}\right). \tag{6}$$

In the temperature range of the non-monotonic shift of the absorption edge, equation (3) can be simplified in several specific temperature ranges (or points) including the low temperature zone (almost no ionization of defects), the middle ionization zone (low density of ionized defects), the strong ionization zone (high density of ionized defects), the transitional zone, and the high temperature intrinsic ionization zone (intrinsic carriers prevailing), based on which the E_F can be expressed by setting $E_v = 0$:

$$E_F = \begin{cases} 0.5\Delta E_A, & \text{(a)} \\ 0.5\Delta E_A - 0.75k_BT_b, & \text{(b)} \\ 0.5\Delta E_A, & \text{(c)} \\ \Delta E_A, & \text{(d)} \\ \Delta E_A + 3.69k_BT_e, & \text{(e)} \\ E_i - k_BT_f\text{arcsh}(N_A/2n_i), & \text{(f)} \\ E_i, & \text{(g)} \end{cases} \tag{7}$$

where ΔE_A is the ionization energy of the shallow acceptor. The intrinsic Fermi level E_i satisfies[13,23]

$$E_i = 0.5E_g + 0.75k_BT\ln\left(\frac{m_p^*}{m_n^*}\right). \tag{8}$$

The (a)–(g) represent the positions of E_F at critical temperatures T_i (i = a–g), i.e., T_a: 0 K with $E_F = (E_v + E_A)/2$; T_b: at the minimum of E_F; T_c: the non-zero temperature point with $E_F = (E_v + E_A)/2$; T_d: with $E_F = E_A$, T_e: with beyond 90% ionization of acceptors; T_f: with intrinsic carrier occurrence, and T_g: with $E_F \simeq E_i$. Note that to the four temperature points T_b–T_e, especially T_d and T_e should be paid attention, because they almost correspond to the ionization temperature range of acceptors, i.e., at T_d the ionization ratio of acceptors reaches 20% and at T_e the ionization ratio of acceptors arrives at 90%, these temperatures can be expressed as

$$T_i = \begin{cases} \dfrac{h^2N_A^{2/3}}{68.33k_Bm_p^*}, \\ \dfrac{h^2N_A^{2/3}}{25.12k_Bm_p^*}, \\ \dfrac{\Delta E_A}{k_B\ln(5N_v/N_A)}, \\ \dfrac{\Delta E_A}{k_B\ln(0.025N_v/N_A)}. \end{cases} \tag{9}$$

Note that N_v is a function of temperature. The density of carriers (holes) can be expressed as

$$p_{0(i)} \simeq \begin{cases} 0.12N_A\exp\left(-\dfrac{10.88\pi m_p^*\Delta E_A}{h^2N_A^{2/3}}\right), \\ 0.25N_A\exp\left(-\dfrac{4\pi m_p^*\Delta E_A}{h^2N_A^{2/3}}\right), \\ 0.2N_A, \\ N_A, \end{cases} \tag{10}$$

where i represents the corresponding temperature point. For n-type HgCdTe, the degeneracy factor $g_D = 2$. Equations (9) and (10) can be deduced as

$$T_i = \begin{cases} \dfrac{h^2N_D^{2/3}}{43.04k_Bm_n^*}, \\ \dfrac{h^2N_D^{2/3}}{15.83k_Bm_n^*}, \\ \dfrac{\Delta E_D}{k_B\ln(3N_c/N_D)}, \\ \dfrac{\Delta E_D}{k_B\ln(0.05N_c/N_D)}, \end{cases} \tag{11}$$

$$n_{0(i)} \simeq \begin{cases} 0.23N_D\exp\left(-\dfrac{6.85\pi m_n^*\Delta E_D}{h^2N_D^{2/3}}\right), \\ 0.50N_D\exp\left(-\dfrac{2.52\pi m_n^*\Delta E_D}{h^2N_D^{2/3}}\right), \\ 0.33N_D, \\ N_D. \end{cases} \tag{12}$$

4.2. Results from the calculation of E_F

The E_F is a function of x, conductivity type, doping level, and ionization energy of defect. We mainly focus on the doping levels from 10^{14} to 10^{17} cm^3 by considering the general density of extrinsic and intrinsic dopants in HgCdTe.[38–40] Figure 14 gives the calculated temperature dependence of the band-edge electronic structure and E_F by taking p-doped $Hg_{0.7}Cd_{0.3}Te$ for example.[36] For comparison, the results of unintentionally-doped n-type HgCdTe are shown, since a similar phenomenon is also observed between the absorption edge energy and the empirical formula. From the figure, we can see

that the material system shows a positive temperature coefficient of E_g, but CB and VB both decrease and E_F almost exponentially increases toward E_i with the increase of temperature. After the acceptors are fully ionized, E_F finally approaches to E_i. As mentioned previously, the range from $\sim T_d$ to T_e is the non-monotonic shift range of the absorption edge.

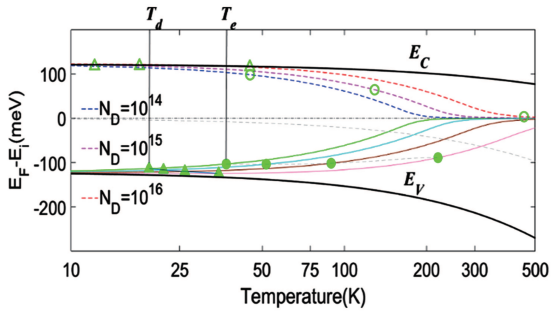


Fig. 14. The evolution of the E_F in p- and n-type HgCdTe with temperature for different parameters (for n-type, $N_D = 10^{14}$–10^{16} cm^{-3}; for p-type, $N_A = 10^{14}$–10^{17} cm^{-3}). Triangles and dots represent the temperature points of T_d and T_e, respectively.

Table 2. Calculated values of the specified temperature points described in E_F function.

Defect activation energy		T/K @ $N_{A/D} \in 10^{14}$–10^{16} cm^{-3} and $x = 0.3$
$E_a(As_{Te}) \sim 10$ meV	T_d	13.6–16.6
	T_e	27.3–68.2
$E_a(V_{Hg}) \sim 15$ meV	T_d	19.3–26.1
	T_e	37.0–89.5
$E_d \sim 3$ meV	T_d	12.2–45.1
	T_e	45.2–454.2

Table 2 gives the predicted results of T_d and T_e in p-type $Hg_{0.7}Cd_{0.3}Te$ under different conditions including doping and activation energies. From the Table, we can see that T_d and T_e increase with doping level (N_A) and ionization energy of acceptors (ΔE_A) increasing,[36] i.e., 13.6 K$< T_d <$ 47.0 K and 27.3 K$< T_e <$ 248.2 K. As discussed above, T_d with $E_F \approx E_A$ can be considered as the initial stage of the ionization of acceptors and T_e as the stage of full ionization of acceptors. In this case, for the As-activated (As_{Te}) $Hg_{0.7}Cd_{0.3}Te$, $N_A = 5 \times 10^{16}$ cm^3 and $\Delta E_{As_{Te}} \approx 10$ meV, the key temperature points can be calculated to be $T_d = 17.0$ K and $T_e = 70.0$ K, which are consistent with the range of the non-monotonic shift of the absorption edge. For V_{Hg}-doped HgCdTe with $x = 0.3$, N_A is on the order of 10^{16} cm^3 and $\Delta E_{V_{Hg}} \approx 15$ meV, the temperature ranges of T_d and T_e are $\sim$ 26–90 K, which are also close to the experimental observations. For the intrinsic n-type $Hg_{0.7}Cd_{0.3}Te$, $N_D = 10^{14}$ cm^3 and $\Delta E_D \approx 3$ meV, the temperature range of T_d and T_e can be deduced to be $\sim$ 15–90 K. Of course, as N_D increases, the range from T_d to T_e should be broadened, and even extended beyond 300 K for T_e. This is consistent with the experimental result, showing that it is difficult to observe the non-monotonic shift of the absorption edge at much higher donor densities due to the very small ΔE_D.

4.3. Influence mechanism of defects on the optical transition

According to the $E_F \sim T$ expression and the experimental data, the temperature-dependent transitions can be explained when extrinsic/intrinsic shallow levels exist in HgCdTe, independent of growth methods and conductivity types, as well as dopant sources. As the experimental observation and the calculated result, the values of T_d and T_e represent the critical points of the non-monotonic shift of the absorption edge, the former corresponding to the occurrence of defect-related transition contribution and the latter for the full contribution of the defect-related transition.

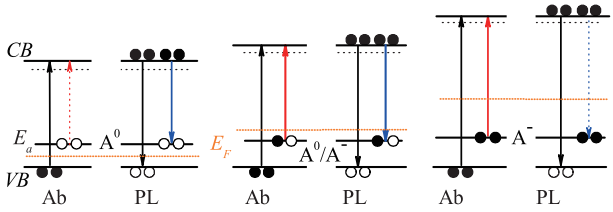


Fig. 15. Schematics for temperature-dependent carrier transition in p-type $Hg_{0.7}Cd_{0.3}Te$ with $E_a \sim 11$ meV and $N_c \sim 1 \times 10^{16}$ cm^{-3}: (a) $T < 26$ K, (b) 26 K$< T <$ 90 K, and (c) $T >$ 90 K.

Thus, a schematic evolution of the carrier transition can be presented by taking a p-type $Hg_{0.7}Cd_{.3}Te$ for example as shown in Fig. 15. The temperature values in the figure refer to the specified parameters of the sample with $E_a \sim 11$ meV at $N_c \sim 1 \times 10^{16}$ cm^{-3}.[24] This figure shows that at low temperature below 26 K (Fig. 15(a)), the carriers in the defect state (holes) are frozen. When the transmission measurement is conducted, only the electrons from the VB are excited to the CB but the states in E_a are localized without activity (i.e., holes are not activated). Here, the absorption edge follows the law of the intrinsic absorption. However, under the PL measurement conditions, the excited electrons in the CB from the VB by lasers can recombine with localized vacancies in the defect state together with holes in the VB. This is also the fact that for detecting defect-related shallow levels, low temperatures are frequently required for PL measurement. As the temperature increases (Fig. 15(b)), the frozen holes in the defect states begin to be thermally activated. In this case, the activated holes in E_a, the anions due to the capture of electrons, can join in the transition of transmission process, which provides a contribution to the absorption edge. Because the transition energy of the defect states is lower than the VB–CB transition energy, the absorption edge energy is red-shifted. As the temperature raises beyond 90 K (Fig. 15(c)), the holes in E_a are almost fully activated and the contribution of their transition to the absorption edge reaches the maximum, and even if the temperature increases further, the influence of the defect states on the absorption edge cannot be increased. As a result, the absorption edge energy follows again the law of the intrinsic absorption; i.e., it almost linearly increases with temperature increasing.

It can also be pointed out that the full activation of E_a at high temperatures means that the defect states can always be occupied by electrons, which can participate in the absorption process to the CB but cannot find electrons from the CB to give rise to emission. This is also the reason why it is difficult to observe a PL signal of shallow defects at high temperatures.

5. Conclusions and perspectives

Intrinsic V_{Hg} doping provides a way to realize p-type HgCdTe, although the carrier density and the mobility are limited. The extrinsic-As doping presents an option for high quality epilayers but specified annealing processes are necessary, such as a two-stage process with a relatively low temperature of 285 °C to activate the As to occupy Te sites and simultaneously to avoid producing the excessive V_{Hg}. Optical characterization by utilizing transmission and PL spectroscopy can optimize the annealing conditions through analyzing the defects generated or eliminated in different annealing processes. After the value of E_g in HgCdTe is determined, the transmission can effectively disclose the band-to-band transition of carriers, but the reference temperature is a main factor in the measurement. This is because defects in HgCdTe can influence the contribution of the band-related carrier transition to the intrinsic absorption edge, which on one hand leads to a non-monotonic shift of the absorption edge energy with temperature increasing in the low temperature range < 100 K, and on the other hand makes the experimental Stokes energy abnormally shift from positive to negative when the temperature is beyond the critical point or the corresponding defect activation energy.

To evaluate the optical E_g of the doped HgCdTe, the absorption should be measured at very low temperatures; e.g., far below 77 K. While for the PL measurement, a much high temperature—e.g., up to ambient temperature—is beneficial to avoid the influence from the defects or the band tail states. The lower activation energy of the As (denoted as As_{Te}) than V_{Hg} points to the advantages of fabricating p-type HgCdTe-devices based on the As-doped HgCdTe after the application of a suitable annealing process.

Acknowledgment

Part of work was done with the help of Prof. J. Shao from the Shanghai Institute of Technical Physics, Chinese Academy of Sciences.

References

[1] Martyniuk P, Antoszewski J, Martyniuk M, Faraone L and Rogalski A 2014 *Appl. Phys. Rev.* **1** 041102
[2] Lei W, Antoszewski J and Faraone L 2015 *Appl. Phys. Rev.* **2** 041303
[3] Li Q, He J L, Hu W D, Chen L, Chen X S and Lu W 2018 *IEEE T. Electron. Dev.* **65** 572
[4] Tomm J W 1994 *Curr. Top. Cryst. Growth Res.* **1** 245
[5] Berding M A, Sher A, Schilfgaarde M V, Chen A C and Arias J 1998 *J. Electron. Mater.* **27** 605
[6] Hu W D, Liang J, Yue F Y, Chen X S and Lu W 2016 *J. Infrared Millim. Waves* **35** 25
[7] Wu J, Xu F F, Wu Y, Chen L, Yu M F and He L 2005 *J. Infrared Millim. Waves* **24** 81
[8] Duan H, Chen X S, Huang Y and Lu W 2007 *Solid State Commun.* **143** 471
[9] Yue F Y, Chu J H, Wu J, Hu Z G, Li Y W and Yang P X 2008 *Appl. Phys. Lett.* **92** 121916
[10] Shao J, Yue F Y, Lü X, Lu W, Huang W, Li Z F, Guo S L and Chu J H 2006 *Appl. Phys. Lett.* **89** 182121
[11] Yue F Y, Wu J and Chu J H 2008 *Appl. Phys. Lett.* **93** 131909
[12] Chu J H, Mi Z Y and Tang D Y 1991 *Infrared Phys.* **32** 195
[13] Chu J H, Xu S C and Tang D Y 1983 *Appl. Phys. Lett.* **43** 1064; Chu J H, Sher A 2007 *Springer-Verlag*
[14] Hansen G L, Schmidt J L and Casselman T N 1982 *J. Appl. Phys.* **53** 7099
[15] Shao J, Lu W, Lv X, Yue F Y, Li Z F, Guo S L and Chu J H 2006 *Rev. Sci. Instrum.* **77** 063104
[16] Cui H Y, Zeng J D, Tang N Y and Tang Z 2013 *Opt. Quant. Electron.* **45** 629
[17] Qiu W, Hu W D, Chen L, Lin C, Cheng X, Chen X S and Lu W 2015 *IEEE T. Electron. Dev.* **62** 1926
[18] Sun L Z, Chen X S, Sun Y L, Zhou X H, Quan Z J, Duan H and Lu W 2005 *Phys. Rev. B* **71** 192303
[19] Yue F Y, Chen L, Li Y W, Sun L, Yang P X and Chu J H 2012 *Chin. Phys. B* **21** 017804
[20] Yue F Y, Shao J, Lü X, Huang W, Chu J H, Wu J, Lin X C and He L 2006 *Appl. Phys. Lett.* **89** 021912
[21] Yue F Y, Shao J, Wei Y F, Lv X, Huang W, Yang J R and Chu J H 2007 *Acta Phys. Sin.* **56** 2878 (in Chinese)
[22] Chu J H, Mi Z Y and Tang D Y 1992 *J. Appl. Phys.* **71** 3955
[23] Chu J H, Li B, Liu K and Tang D Y 1994 *J. Appl. Phys.* **75** 1234
[24] Yue F Y, Chen L, Li Y W, Hu Z G, Sun L, Yang P X and Chu J H 2010 *Chin. Phys. B* **19** 117106
[25] Yue F Y, Chen L, Wu J, Hu Z G, Li Y W, Yang P X and Chu J H 2009 *Chin. Phys. Lett.* **26** 047804
[26] Hu W D, Chen X S, Ye Z H, Chen Y G, Yin F, Zhang B and Lu W 2012 *Appl. Phys. Lett.* **101** 181108
[27] Hu W D, Ye Z H, Liao L, Chen H L, Chen L, Ding R J, He L, Chen X S and Lu W 2014 *Opt. Lett.* **39** 5184
[28] Li Y T, Hu W D, Ye Z H, Chen Y Y, Chen X S and Lu W 2017 *Opt. Lett.* **42** 1325
[29] Hu W D, Chen X S, Ye Z H, Feng A L, Yin F, Zhang B, Liao L and Lu W 2013 *IEEE J. Sel. Top. Quant. Electron.* **19** 4100107
[30] Boieriu P, Chen Y and Nathan V 2002 *J. Electron. Mater.* **31** 694
[31] Berding M A, van Schilfgaarde M and Sher A 1994 *Phys. Rev. B* **50** 1519
[32] Sun L Z, Chen X S, Zhao J J, Wang J B, Zhou Y C and Lu W 2007 *Phys. Rev. B* **76** 045219
[33] Vydyanath H R and Hiner C H 1989 *J. Appl. Phys.* **65** 3080
[34] Edwall D, Piquette E, Ellsworth J, Arias J, Swartz C H, Bai L, Tompkins R P, Giles N C, Myers T H and Berding M 2004 *J. Electron. Mater.* **33** 752
[35] Shi X H, Rujirawat S, Ashokan R, Grein C H and Sivananthan S 1998 *Appl. Phys. Lett.* **73** 638
[36] Wang H, Hong J, Yue F Y, Jing C B and Chu J H 2017 *Infrared Phys. Techn.* **82** 1
[37] Shao J, Lu W, Yue F Y, Lv X, Huang W, Li Z F, Guo S L and Chu J H 2007 *Rev. Sci. Instrum.* **78** 013111
[38] Selamet Y, Grein C H, Lee T S and Sivananthan S 2001 *J. Vac. Sci. Technol. B* **19** 1488
[39] Kenworthy I, Capper P, Jones C L, Gosney J J G and Coates W G 1990 *Semicond. Sci. Technol.* **5** 854
[40] Grein C H, Garl, J W, Sivananthan S, Wijewarnasuriya P S, Aqariden F and Fuchs M 1999 *J. Electron. Mater.* **28** 789